Electrical conductivity of nonideal carbon and zinc plasmas: Experimental and theoretical results

J. Haun and H.-J. Kunze
Institut für Experimentalphysik V, Ruhr Universität Bochum, 44780 Bochum, Germany

S. Kosse and M. Schlanges
Institut für Physik, Ernst-Moritz-Arndt Universität Greifswald, Domstrasse 10a, 17489 Greifswald, Germany

R. Redmer
Universität Rostock, Fachbereich Physik, 18051 Rostock, Germany
(Received 19 June 2001; published 26 March 2002)

Electrical conductivities of nonideal carbon and zinc plasmas have been measured in this paper. The plasma is produced by vaporizing a wire placed in a glass capillary within some hundred nanoseconds. In the case of carbon, vaporization occurs with good reproducibility when utilizing a preheating system. The particle density is in the range of $n=(1-10)\times 10^{21}$ cm^{-3}. The plasma temperature, which is obtained by fitting a Planck function to the measured spectrum, is between 7–15 kK. Plasma radius and behavior of the plasma expansion were studied with a streak, a framing or an intensified charge coupled device camera. We compare the measured electrical conductivities with theoretical results, which were obtained solving quantum kinetic equations for the nonideal partially ionized plasmas. In this approach, the transport cross sections are calculated on the level of a *T*-matrix approximation using effective potentials. The plasma composition is determined from a system of coupled mass action laws with nonideality corrections.

DOI: 10.1103/PhysRevE.65.046407 PACS number(s): 52.25.Fi, 52.25.Jm, 52.80.Qj, 05.60.−k

I. INTRODUCTION

The study and the understanding of transport mechanisms of nonideal plasmas has become more and more important in recent decades. A fundamental quantity that can be measured is the electrical conductivity. Theories for ideal plasmas or conducting liquids of Spitzer [1] and Ziman [2], respectively, are not capable of describing the behavior of such plasmas. The models of Lee and More [3], and Djuric [4] also do not fit with the experimental values very well. Theoretical improvements require a more rigorous approach to the transport properties of nonideal plasmas based on quantum statistical theory. Such investigations have been done in the recent years in the frame of kinetic theory and linear response theory (see, e.g., [5–13]).

To conceive a better understanding of the processes in nonideal plasmas, it is important to have as many different methods of measurements as possible as well as an appropriate theoretical description of the regime of nonideal partially ionized plasmas. Measurements of the electrical conductivity were carried out by Benage for polyurethane and aluminum [14,15], and experimental data for copper and aluminum plasmas were published by DeSilva and coworkers [16–18]. For tungsten several different measurements were performed and modeled by Kloss and coworkers [19–22]. These measurements allow a comparison with theoretical results for the electrical conductivity, e.g., obtained with the linear response theory for metal plasmas [23,24]. In this paper we compare the latest measurements of carbon and zinc plasmas with the results of the kinetic theory for partially ionized plasmas.

New technologies based upon laser and particle beams, *x*-ray lasers, and plasma sources, e.g., the very efficient cluster lamps [25] and flash lamps, advance the research of nonideal plasmas. Arrays of some hundred tungsten wires are simultaneously vaporized in new ultra high power *x*-ray lamps (200 TW) for fusion applications [26]. The electrical conductivity of these nonideal plasmas determines the efficiency of such arrangements. Nonideal plasma occurs when matter is subjected to strong shock, detonation, and electric explosion waves, and during hypersonic motion of bodies in dense planetary atmospheres. In nature nonideal plasmas can be found in the core of dwarf stars or giant gaseous planets, such as, jupiter [27], or in the core of a lightning stroke.

Nonideal plasmas are characterized by the coupling parameter Γ, which is defined as the ratio of the mean potential energy to the mean kinetic energy: $\Gamma=(\langle Z\rangle^2 e^2)/(4\pi\epsilon_0 k_B T r_i)$, with the ion sphere radius $r_i=\sqrt[3]{3/4\pi n_i}$ and the average ionization level $\langle Z\rangle$. Obviously $\Gamma\propto\sqrt[3]{n_i}/T$ and is therefore given by the ion density n_i and the temperature T. With respect to the following measurements, we estimate a maximum ionization level of $\langle Z\rangle=1$. In general the ionization level is $\langle Z\rangle<1$ in our measurements. For $\Gamma\lesssim 1$, we have a weakly nonideal plasma. For $\Gamma>1$ the plasma is nonideal or strongly coupled. In our plasmas the coupling parameter is in the range of $0.3<\Gamma<2.6$.

We produce the nonideal plasma at near-solid-state densities and temperatures lower than 16 000 K by fast vaporization of a metal wire, often called an exploding wire. The wire is surrounded by a small duran-glass capillary. The capillary confines the plasma column for some hundred nanoseconds before it disintegrates. by using this technique one has the following three advantages: First the plasma reaches a higher density because the expansion process is stopped by the capillary. Second the homogeneity is better, and third the kink and sausage instabilities are reduced. The combination of different capillaries and wire diameters allows us to produce homogeneous plasmas in a wide range of densities and temperatures.

In all previous exploding wire experiments only metallic or metal-like wires were vaporized. The reason for this is the good electrical conductivity of metals. The resulting fast energy input leads to a well reproducible and homogeneous plasma. On the other hand the conductivity of carbon is three orders of magnitude smaller than that of metals. Therefore it was not possible to produce good carbon plasmas in the past. In contrast to metals, the conductivity of carbon increases with increasing temperature (hot conductor). Therefore, developing a preheating system enabled us to use this effect for producing carbon plasmas with the same homogeneity and reproducibility as it is seen for metal plasmas. We chose carbon because it is the lightest (and therefore simple to describe) element, which is solid at room temperature and also easy to handle. Carbon is a very important element in nature and in technical applications. Zinc is interesting due to its low melting point and because the metal-nonmetal transition called ''Mott's transition'' [28] is predicted completely inside the liquid phase [29].

This paper is organized as follows. The experimental setup is described in Sec. II. In Sec. III we explain the production of the plasmas, describe the preheating system and the measurements of the temperature. We present the kinetic approach to the electrical conductivity in Sec. IV using standard methods of kinetic theory. We determine the plasma composition from a coupled system of mass action laws. The transport cross sections are calculated in the *T*-matrix approximation. In Sec. V, we compare the measured conductivities with our theoretical results.

II. EXPERIMENTAL SETUP

A carbon wire with diameter of 273 μm, or a zinc wire with diameter of 125 μm or 380 μm was inserted into a duran glass capillary of 24 mm in length, having an inner diameter ranging from 0.4 to 1.3 mm and an outer diameter ranging from 6.0 to 9.0 mm. The size of the wire was small enough to guarantee homogeneous vaporization without impairment due to the skin effect. On the other hand, due to the high electric field surrounding the wire at the beginning, the generation of a peripheral discharge could be induced if the diameter of the wire was too small. Sparks at the ends of the electrodes were avoided by soldering the wire to the electrodes (especially for the brittle material carbon). A (1/4)-m monochromator equipped with a photomultiplier observed the plasma to provide a monitor signal. Sparks or contact problems of particular shots could be recognized when using this technique. The wire surrounded by the glass capillary was placed in a discharge chamber 30 cm in diameter. Six windows in the chamber enabled us to observe the plasma. The arrangement of the two electrodes is shown in Fig. 1. Two low inductive capacitors connected in parallel are charged up to $U=20$ kV and discharged through the wire by closing a low inductive pressurized spark gap switch. The maximum energy stored in the capacitor bank ($C=3.86$ μF) was 770 J. The small resistance of 27 $m\Omega$ and the low inductance of only 154 nH of the circuit make sure that the current rises to a first peak of 12 kA within 200 ns with the zinc wire and to a peak of 34 kA within 1500 ns

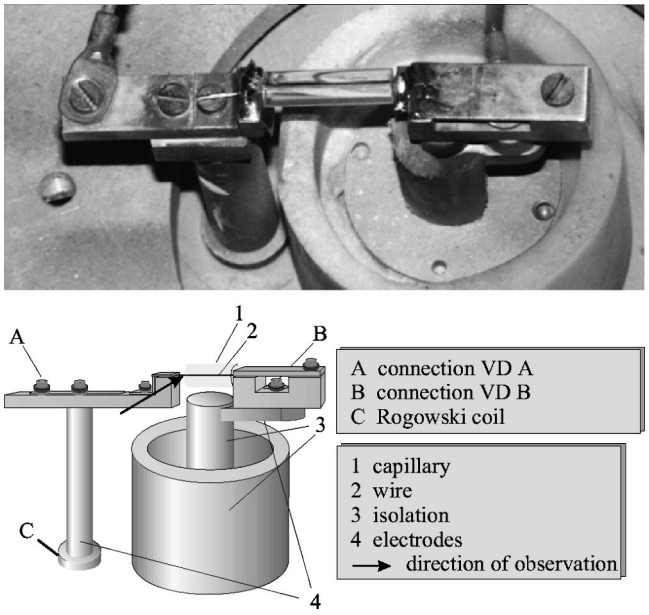

FIG. 1. Top: Photo of the wire inside the capillary connected to the electrodes; below: Schematic drawing of the arrangement.

with the carbon wire. A separately calibrated Rogowski coil surrounds one electrode to measure the time derivative of the current. The current itself is obtained by integration of the Rogowski signal. To check the calibration of the Rogowski coil the total charge calculated by integrating the current over the time is compared with the original charge on the capacitor bank $Q=UC$ minus the remaining charge after the discharge. The resulting error is smaller than 1%. Two voltage dividers, each consisting of a 3-kΩ resistor (three 1 kΩ 2 W carbon resistors in series) in series with a 50-Ω resistor are used to measure the voltage at the load. The 50-Ω resistor consists of eight 400-Ω resistors in parallel, mounted in a low inductance configuration. The calibration of the voltage dividers was done very carefully for a wide frequency range from 50 Hz to 20 MHz, and it turned out that in this range the inductive or capacitive components can be neglected. The measured voltage consists of a resistive and an inductive component $U=IR+d/dt(LI)$. During the first 50 ns the resistance of the wire and dL/dt are both small enough so that the IR and IdL/dt terms are negligible relative to the LdI/dt term, and the wire inductance L may be determined as the ratio of voltage to the current time derivative. This checks well the calculated inductance of a cylindrical conductor. Later the resistive component dominates. Since the change in inductance due to phase transitions is negligibly small, solving for the plasma conductivity σ yields

$$\sigma=\frac{l}{RA}=\frac{I}{U-L_D\dot{I}}\frac{l}{\pi r^2}, \tag{2.1}$$

where A and r are cross sections and radius of the plasma column, respectively, and L_D is its inductance. r was measured in different ways. First we employed an IMACON camera, which can be used either in a streak or in a framing mode. For streak pictures the wire image was focused onto

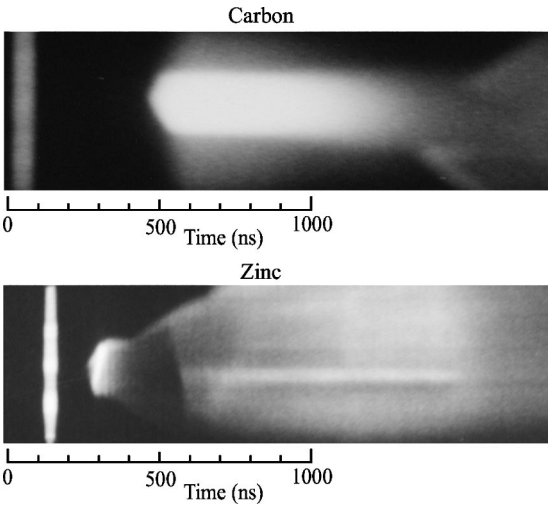

FIG. 2. Typical streak pictures of carbon and zinc plasmas. The time mark (vertical line) of the ruby laser can be seen on the left margin of the pictures. The plasma light emission starts at 450 ns for carbon and at 250 ns for zinc. The plasma is reaching the inner part of the capillary (0.78 mm at carbon, 0.73 mm at zinc) very quickly. Then the capillary fixes the plasma radius some hundred nanoseconds for carbon and about hundred nanoseconds for zinc before it breaks. The light emission is reduced at this moment for zinc. Conductivities are measured after the plasma has reached the inner part of the capillary and before the capillary breaks.

the entrance slit oriented perpendicularly to the wire. We used streak speeds of 10 to 50 ns/mm on the picture. To fix the time of the streak picture relative to the electrical signals, the pulse of a ruby laser was used. The laser was fired at a short time before the start of the discharge and illuminated the entrance slit thus setting a time mark on the picture. The electrical signal of a fast photodiode observing the laser pulse was recorded on the oscilloscope and gave the time origin of the electrical signals. Two typical streak photos are shown in Fig. 2. For the purpose of taking two-dimensional pictures of the plasma column the entrance slit was removed and the camera was operated in the framing mode. In this mode we obtain 6–20 pictures of one single discharge. The exposure time of each picture is 40 ns and the time between two pictures is 200 ns. The framing pictures also give us information about instabilities, inhomogeneities, the behavior of the plasma column at the ends of the capillary, and possible sparks at the electrodes due to contact problems. Second an intensified charge coupled device (ICCD) camera was used instead of the IMACON camera. The ICCD camera produces one picture (duration 20 to 40 ns) per shot of the whole wire with high quality. The plasma column was observed inside one single capillary as well as in the gap between the two parts of a capillary that has been cut in two pieces. The capillary acts like a lens for light originating in the middle of the capillary. Different magnification of the plasma column at the detector is the result. With the help of the framing camera and the ICCD camera, it is possible to obtain the different magnification factor and to record the behavior of the plasma inside and outside the capillary.

The spectral density profile is observed within the range 400 nm$<\lambda<$700 nm with the help of a (1/8)-m spectrograph and an optical multichannel analyzer. The gate time was 30–100 ns and the spectral resolution was 0.5 nm per channel.

III. DATA ANALYSIS

A. Production of the carbon plasma

Compared to metals the electrical conductivity of carbon is three orders of magnitude smaller at room temperature. Therefore, the energy input is too slow to produce a homogeneous plasma, without kink or sausage instabilities. The conductivity increases with temperature. As written in Forsythe [30] the conductivity rises from 2.9×10^4 $(\Omega\mathrm{m})^{-1}$ at $T=0\,^\circ\mathrm{C}$ to 1.1×10^5 $(\Omega\mathrm{m})^{-1}$ at $T=2500\,^\circ\mathrm{C}$. These values can only be taken as a tendency, because the exact behavior of the conductivity strongly depends on the lattice structure of the carbon used for the experiments. The fact of higher conductivity at high temperature is used for developing a preheating system. A dc current of 1 A heats the wire in 0.8 s to about 3000 K. The period is long enough to heat the wire homogeneously but short enough not to loose material from the wire by oxidation. Various experiments were carried out to find optimum conditions. After preheating, the main discharge is triggered automatically and the wire starts to vaporize. To prevent the destruction of the dc power supply, connected in parallel to the main capacitor bank, two high inductance coils and some diodes were installed in the circuit of the dc power supply.

Figure 3 shows framing pictures of typical discharges. The instabilities occur more extensively if the capillary is absent, because the capillary wall suppresses instabilities as soon as the plasma reaches the inner wall of the capillary. Therefore, instabilities can be observed better in explosions in air. If a random hot channel develops, the conductivity increases more inside the hot channel than in other zones of the wire due to the ''hot conductor characteristic'' of carbon. As a result the channel heats up further and the inhomogeneity grows (self-amplification). For this reason it was not possible to produce homogeneous carbon plasmas in the past by using the exploding wire technique. In this paper we present framing pictures with very homogeneous carbon plasmas. We also vaporized other pure metals (Al, Fe, Ag, Cu, W) in our facility. In comparison to metals the carbon plasma is indeed more homogeneous. As a side effect, sparks at the electrodes, as a result of bad electrical contact, were reduced by the use of the dc precurrent. As a third difference the plasma emits light about 500 ns earlier with the preheating system turned on.

B. Characteristics of the discharge

Figure 4 shows some characteristics of the discharge of carbon and zinc. The different behavior of the discharge can be seen in the current and voltage signals [Figs. 4(a) and 4(b)]. In Figs. 4(c) and 4(d) the resistance and the energy input is shown. The energy is calculated simply by

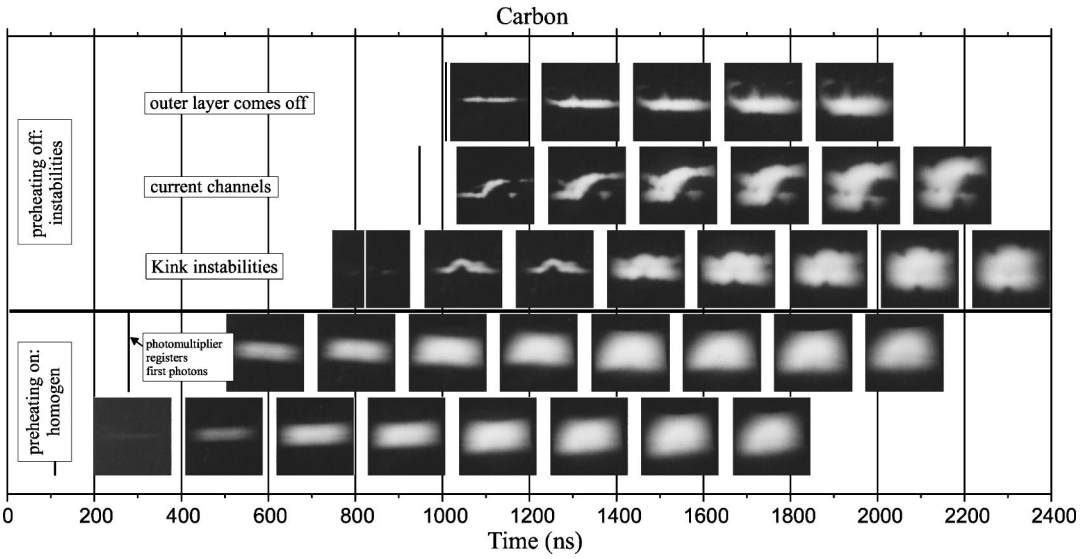

FIG. 3. Framing pictures of the exploding carbon wire in air without capillary. The behavior of the exploding plasma can be studied better without using the capillary. The first three rows show different inhomogeneities as they appear without the preheating system. We observe outer shelters coming off, single current channels, and kink instabilities. The last two rows show perfect homogeneous plasmas. They are as good as plasmas produced from metal wires. With the preheating system switched on, first the plasma has a higher energy before the main discharge is triggered and second the current rises faster because of the higher conductivity of the hot wire. As a consequence the plasma starts to emit light about 0.5 μs earlier.

$$E = \int U(t)I(t)dt. \tag{3.1}$$

Any losses by radiation can be neglected because the radiated power at 10 000 K is orders of magnitude smaller than the energy input according to the Stefan-Boltzmann law. With carbon 200 ns after the beginning the current and the voltage drop; this may be due to the phase transitions. After that the resistance is falling while the plasma state is reached. The plasma is expanding with $v = 3$ km/s and reaches the inner part of the capillary at about 500 ns. The scenario is quite different with zinc: after a first peak in the first 80 ns we observe a dramatic increase of the resistance by about two orders of magnitude. The resulting decrease of the cur-

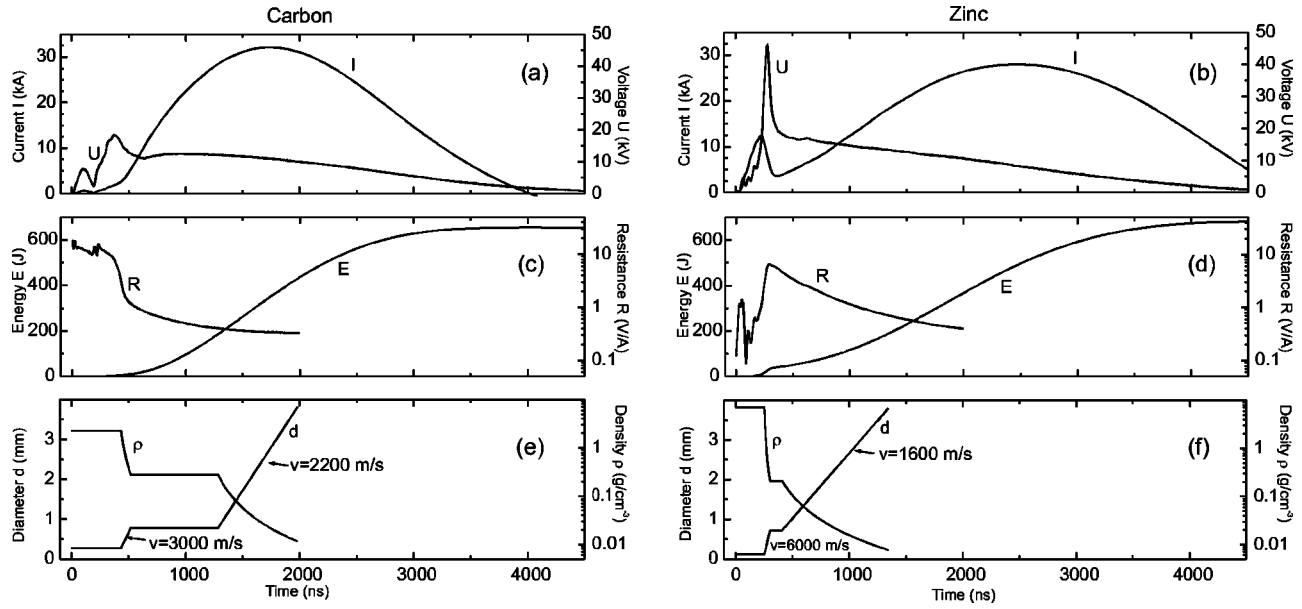

FIG. 4. Measured time traces of the current and voltage for carbon (a) and zinc (b). The resulting resistance and energy put into the wire for carbon (c) and zinc (d). The energy was calculated in 5 ns steps by integrating *UI* over time. The diameters of the wire seen with the streak camera and the resulting particle density are shown for carbon (e) and zinc (f). Pictures (a)–(d) result from the average of many shots. The results of (e)–(f) were obtained from the shots of Fig 2.

rent is prevented by the inductance of the whole circuit. The high energy still stored on the capacitor bank at this time is responsible for the measured increasing voltage. The velocity of the plasma propagation to the capillary wall is higher by a factor of 2 due to the larger voltage at this moment. The voltage peak (46 kV) even exceeds the initial charging voltage of the capacitors (20 kV). At this time the plasma has already reached the inner wall of the capillary. Later at the very end of the discharge, the resistances of carbon and zinc tend to the same magnitude.

The conductivity is measured after the plasma has reached the inner wall of the capillary. The wall guarantees best homogeneity and reproducible plasma parameters. The plasma expansion is stopped for a short time by the capillary wall and the radius is constant as can be seen in Figs. 4(e) and 4(f). The pressure taken from the SESAME [31] table at this moment for the measured density and temperature is about 15 kbars. With carbon the capillary can stop the expansion process for about 800 ns. The conductivity can be measured as a function of temperature for constant density. For zinc [Fig. 4(f)] this time interval is short (80 ns). The change in temperature is smaller than the statistical error of the temperature measurement. Therefore, the conductivity is measured for one temperature at one density. The density of the zinc plasmas is varied by using different capillaries with different inner diameters.

Small disturbances of the density propagate with the local sound speed c_s and therefore expansion will be homogeneous in the case $c_s t < a$ (a is the radius of the channel, t is the characteristic time for the process). In our case t is the time the plasma needs to reach the inner wall of the capillary after the wire has completely vaporized (85 ns for carbon and 50 ns for zinc). In both cases this inequality is fulfilled and hence the plasma should be homogeneous.

C. Temperature measurements

The temperature is measured spectroscopically by fitting a Planck function to the measured spectrum. If homogeneity and local thermodynamic equilibrium (LTE) are assumed and the optical depth $\tau(\lambda,t)$ is higher than 4, the spectral radiation reaches the Planck curve with a small deviation of 2% [32]. This optical depth is reached even at the surface of the plasma. The validity of LTE requires checking relevant time constants and estimating the electron collisional rates [33]. Both plasmas are sufficiently dense and long lived. Also the homogeneity criterion is fulfilled during the whole measuring process and even shortly after the capillary breaks. Only at the very end of the discharge absorption, lines in the spectrum appear coming from a cold outer layer of the plasma. During the relevant period of the discharge, neither the sputtered electrode material (we do not measure close to the electrode) nor the surrounding air disturbs the plasma spectrum or substantially pollutes the plasma. As a result, evacuation of the discharge chamber yields no advantage. In Fig. 5 several ICCD pictures are shown. The emission intensity for zinc is much lower inside the capillary at the beginning of the discharge than for carbon [Figs. 5(d) and 5(a)]. Note that the exposure time of picture in Fig. 5(d) is extended by a factor of 5 and it was taken at a later time of the discharge. One reason is the big diameter of the zinc wire used here (0.38 mm instead of 0.125 mm). But also with thin wires the intensities from zinc plasmas are low. We cut the capillaries into two parts to have higher intensity on the one hand and to see whether the plasma was cooled by the capillary on the other hand. Our measurements show that a cooling of the outer plasma layer by the capillary is not substantial. The measured temperatures in the gap between and inside the capillary were the same within the statistical error as long as the plasma radius is the same.

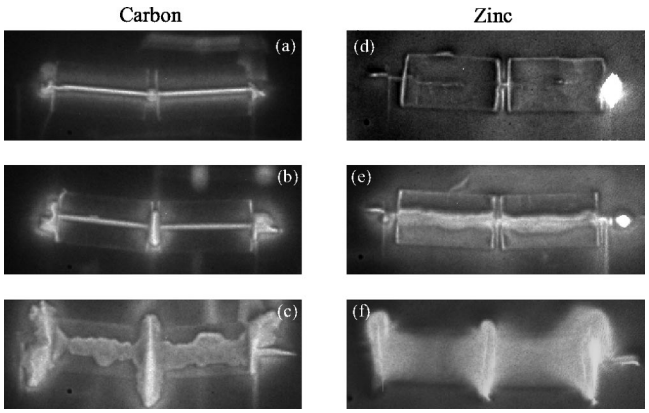

FIG. 5. ICCD pictures of carbon and zinc plasmas. Each picture is taken from a different shot. The pictures show the complete capillaries and a part of the electrodes left and right. Length of the arrangement is about 3 cm. Inside the capillaries we see the carbon and zinc plasmas. We also see the plasma containing the sputtered electrode material at the very end. In this measurement the capillaries were cut into two parts to measure the spectrum in the gap. Exposure time for carbon is 10 ns and for zinc is 50 ns. The figures were taken at (a) 550 ns, (b) 615 ns, (c) 1210 ns, (d) 770 ns, (e) 1095 ns, (f) 1950 ns.

On the ICCD pictures we can see again the good homogeneity inside the capillary for carbon until the capillary breaks [Figs. 5(a) and 5(b)]. However, we see a plasma coming from the electrode material especially in the zinc case. Therefore we measured the spectrum only in the center plane of the plasma column. The effect of the capillaries is clearly demonstrated in these pictures: without the capillary the whole plasma column would expand as observed in the gap between the capillaries. With the help of the capillaries the confinement time of the plasma is increased and as a consequence the density is much higher in contrast to exploding wire experiments done in air. This effect is more extensive for carbon than for zinc. The same behavior can also be seen in the framing pictures (Fig. 6). Here we used the thin zinc wires (0.125 mm).

In Fig. 7 the results of the temperature measurements are shown. Because the radius of the plasma is constant for a long time after reaching the inner part of the capillary, the temperature is given as a function of time. In the zinc case the radius is constant only for a very short moment. Therefore we used different capillaries to vary the density. The temperature is given as a function of the density. The error in

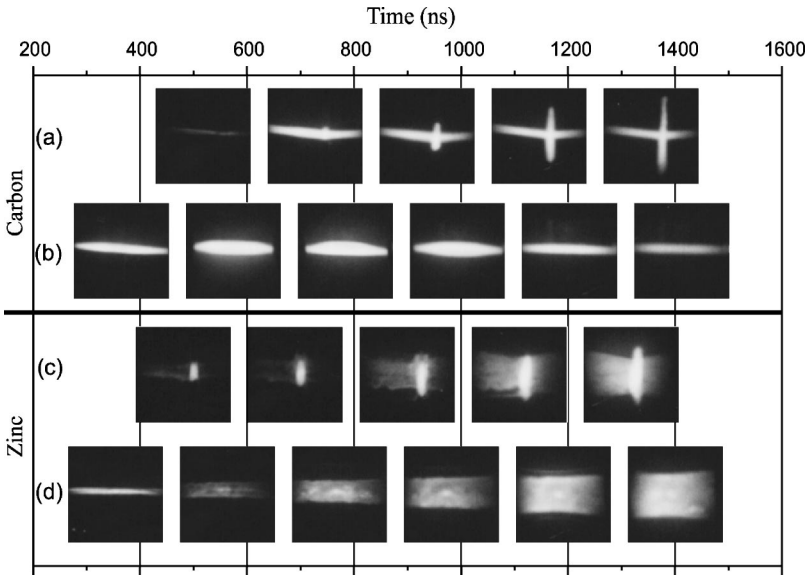

FIG. 6. Framing pictures of carbon and zinc plasmas. The advantage of the framing camera is that each row covers one single shot. The windows show an area of about 1.5 cm^2. Exposure time of each shot is 40 ns. Time between two pictures is about 200 ns. In figures (a) and (c) the capillaries are cut into two parts and the gap between the capillary parts can be seen.

both cases is the statistical error of many shots.

To have an estimation of the difference between the electron temperature T_e and the gas temperature T_g we use the relation from Finkelnburg and Maecker [34] for steady discharges:

$$\frac{T_e - T_g}{T_e} = \frac{m_s}{4\ m_e} \frac{(\lambda_e e E)^2}{\left(\frac{3}{2} k_B T_e\right)^2} \ll 1. \tag{3.2}$$

In this equation $(\lambda_e e\, E)$ is the energy that an electron (mass m_e) acquires from the electric field during one mean free path λ_e. For m_s we take the mass of one zinc or carbon atom. The mean free electron path is calculated with the help of the measured conductivity $\sigma = e\, n_e \mu_e$. The electron mobility μ_e can be calculated with the help of the Boltzmann collision equation and we obtain

$$\lambda_e = \frac{8}{3} \frac{\sigma}{e^2 n_e} \sqrt{\frac{2 m_e k_B T_e}{\pi}} \approx 3 \times 10^{-10}\ \text{m}. \tag{3.3}$$

As a result we may conclude that the electron temperature and the gas temperature are nearly equal in our plasmas, $\Delta T / T_e \approx 0.1\%$.

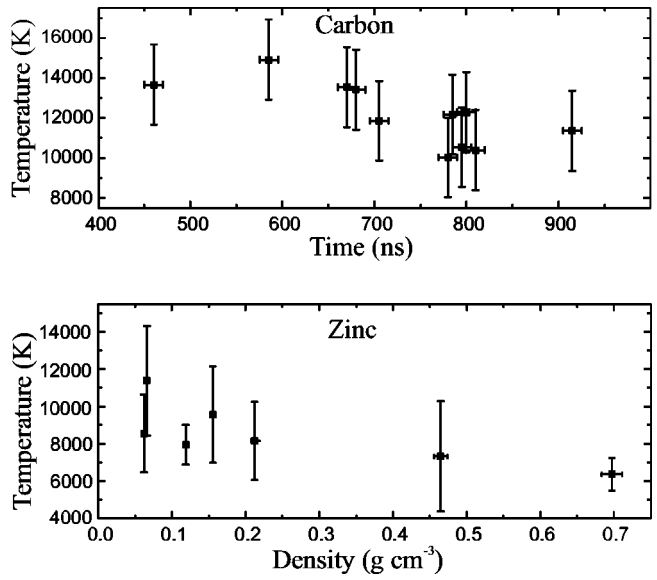

FIG. 7. Measured temperatures of carbon and zinc plasmas. For carbon the temperature is given as a function of time. The radius and density are constant $\rho = 0.28\ \text{g cm}^{-3}$. For zinc the temperature is given as a function of the density. The error given here is the statistical error of many shots.

IV. KINETIC APPROACH TO CONDUCTIVITY

In this section we present a kinetic approach to obtain theoretical electrical conductivities of carbon and zinc plasmas. The plasmas produced in the experiments are considered to be partially ionized. For their theoretical description, we employ the so-called chemical picture, i.e., the plasma species are electrons, ions and atoms with number densities n_e, n_Z, and n_0. The ions in the charge state Z and the atoms are assumed to be in the ground state. Furthermore, we consider a spatially homogeneous plasma at temperature T in a constant electric field $\mathbf{E}$.

In the frame of kinetic theory the electrical current density can be calculated from

$$\mathbf{j} = e \int \frac{d^3 p_e}{(2\pi\hbar)^3} \frac{\mathbf{p}_e}{m_e} f_e(\mathbf{p}_e) = \sigma \mathbf{E}, \tag{4.1}$$

where σ is the dc electrical conductivity. In order to determine the electron distribution function f_e we start from the quantum Boltzmann kinetic equation for a multicomponent system [35–37]. In the nondegenerate case, it follows

$$e\mathbf{E}\cdot\boldsymbol{\nabla}_{\mathbf{p}_e} f_e(\mathbf{p}_e)$$

$$= \frac{1}{\hbar V}\sum_b \int \frac{d^3p_b}{(2\pi\hbar)^3}\frac{d^3p'_e}{(2\pi\hbar)^3}\frac{d^3p'_b}{(2\pi\hbar)^3} \times |\langle \mathbf{p}_e\mathbf{p}_b|\mathrm{T}_{eb}|\mathbf{p}'_b\mathbf{p}'_e\rangle|^2 2\pi\delta(E_{eb}-E'_{eb}) \times\{f_e(\mathbf{p}'_e)f_b(\mathbf{p}'_b)-f_e(\mathbf{p}_e)f_b(\mathbf{p}_b)\}. \quad (4.2)$$

On the (rhs) right-hand side there are the different collision terms where b labels the plasma species. We account for the electron-electron scattering and elastic scattering processes of the electrons with the ions and the atoms on the level of T-matrix approximations. Here, E_{eb} denote the energies and $\langle|T_{eb}|\rangle$ are the T matrices.

In the case of small deviations from thermodynamic equilibrium, standard methods of transport theory can be used to calculate the electrical conductivity [13,38,39]. We utilize the Sonine polynomial expansion of the distribution function and get for the nth order approximation of the electrical conductivity

$$\sigma^{(n)} = \frac{3\sqrt{\pi}}{8}\frac{n_e e^2}{\sqrt{2m_e k_B T}}\frac{\Delta I_0^{(n)}}{\Delta I^{(n)}} \quad (4.3)$$

with the determinants

$$\Delta I_0^{(n)} = \begin{vmatrix} I^{11} & \cdots & I^{1n} \\ \vdots & & \vdots \\ I^{n1} & \cdots & I^{nn} \end{vmatrix} \quad \text{and} \quad \Delta I^{(n)} = \begin{vmatrix} I^{00} & \cdots & I^{0n} \\ \vdots & & \vdots \\ I^{n0} & \cdots & I^{nn} \end{vmatrix}.$$

According to the rhs of Eq. (4.2) we have $I^{\nu\mu}=\Sigma_b I_{eb}^{\nu\mu}$. The expressions for the $I_{eb}^{\nu\mu}$ follow in known manner by inserting the Sonine polynomial expansion in the collision terms. For example, the electron-ion and the electron-atom contributions take the form

$$I_{eb}^{\nu\mu} = n_b \int dz Q_{eb}^T(z) S_{3/2}^{\nu}(z) S_{3/2}^{\mu}(z) e^{-z^2}, \quad (4.4)$$

where $S_{3/2}^{\nu}$ are the Sonine polynomials and $z^2=p^2/2m_e k_B T$. The transport cross sections are given by $(m=1)$

$$Q_{eb}^T = 2\pi\int_0^{\pi} d\vartheta \sin\vartheta(1-\cos^m\vartheta)\sigma_{eb}, \quad (4.5)$$

with σ_{eb} being the differential cross sections in T-matrix approximation. The expression $I_{ee}^{\nu\mu}$ that follows from the electron-electron collision term can be written as

$$I_{ee}^{\nu\mu} = n_e\sqrt{2}\sum_{s=1}^{\nu+\mu-1}\int_0^{\infty} dz A_s^{\nu\mu} z^{2s+5} Q_{ee}^T e^{-2z^2}. \quad (4.6)$$

Here, the transport cross sections are given by Eq. (4.5) with $m=2$ (for $\nu+\mu<6$). The coefficients $A_s^{\nu\mu}$ can be found, e.g., in Ref. [40].

Two problems have to be solved to calculate the electrical conductivity from Eq. (4.3): (i) The quantum mechanical cross sections have to be calculated, and (ii) the composition of the nonideal partially ionized plasma has to be determined.

For plasmas, as considered in this paper, the calculation of the cross sections is a rather difficult problem. In fact, the scattering of electrons on ions and atoms with many bound electrons embedded in a dense nonideal plasma has to be treated, i.e., both the complicated ionic and atomic structure as well as plasma medium effects have to be taken into account. For an approximate treatment various interaction models were considered in the recent years to calculate scattering quantities for the determination of the electrical conductivity of such nonideal plasmas (see, e.g., [6,13]). Here, we will use a simplified approach, i.e., we describe the scattering processes using analytic effective two-body potentials where plasma screening is included in the static limit. Thus, the electron-electron and the electron-ion interactions are described by statically screened Coulomb potentials

$$V_{eb}(r) = -\frac{1}{4\pi\varepsilon_0}\frac{e\,e_b}{r}e^{-\kappa r}. \quad (4.7)$$

Here, e_b denotes the charge of species b. In the nondegenerate case, the inverse screening length is $\kappa=(n_e e^2/k_B T\varepsilon_0)^{1/2}$. For the electron-atom interaction, we use the model of a screened polarization potential given by [41]

$$V_{eb}^{pol}(r) = -\frac{\alpha_D}{2}\frac{e^2}{4\pi\varepsilon_0}\left(\frac{1+\kappa r}{r^2+r_0^2}\right)^2 e^{-2\kappa r}, \quad (4.8)$$

where α_D is the ground-state polarizability with the values $\alpha_D=1.76\times10^{-24}$ cm^3 for carbon and $\alpha_D=7.1\times10^{-24}$ cm^3 for zinc [42]. For the cutoff parameter r_0, which determines the behavior at small distances, we use the relation $r_0^4=\alpha_D\times a_B/2Z_A^{1/3}$ [43] with a_B being the Bohr radius and Z_A being the atomic number. In order to calculate the cross sections for the different scattering processes, their representation in terms of the scattering phase shifts was used [43–45]. The phase shifts were calculated by numerical solution of the corresponding Schrödinger equations with the interaction potentials given by Eqs. (4.7) and (4.8). To demonstrate the behavior of the cross sections, respective results for a carbon plasma are shown in Figs. 8 and 9. In Fig. 8 the transport cross section of $e-C^+$ scattering is displayed as a function of the wave number for different values of the inverse screening length. We observe a lowering with increasing plasma screening. Furthermore, resonance states appear leading to typical structures in the low energy range. A comparison of cross sections for the different scattering processes is presented in Fig. 9. Electron-atom scattering gives the lowest contribution whereas higher cross sections follow from the scattering of electrons on electrons and ions in higher charge states. The behavior of the resonance states in the electron-ion scattering can be seen clearly.

To model the plasma composition we consider ionization and recombination processes according to $X_{Z-1}\rightleftharpoons X_Z+e$. Assuming the stage where chemical equilibrium is reached, the composition of the plasma is determined by the well-known condition

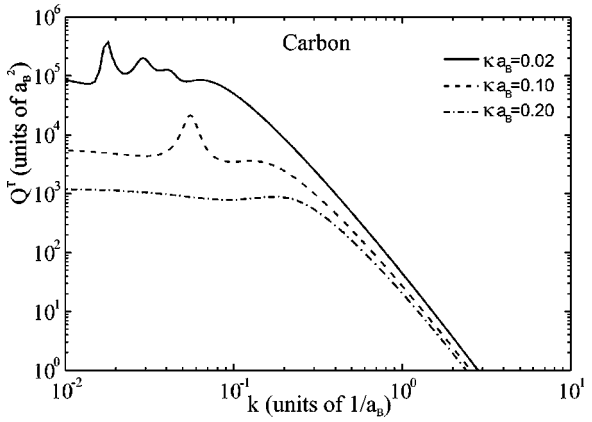

FIG. 8. Transport cross sections for $e-C^+$ scattering in T-matrix approximation vs the wave number for different screening parameters κa_B. $\kappa=(n_e e^2/k_B T\varepsilon_0)^{1/2}$ is the inverse screening length and a_B is the Bohr radius.

$$\mu_{Z-1}=\mu_Z+\mu_e. \tag{4.9}$$

Here, μ_e is the chemical potential of the electrons and μ_Z that of the ions in the charge state Z (μ_0 corresponds to the atoms). We divide the chemical potential according to $\mu_b=\mu_b^{id}+\mu_b^{corr}$, where μ_b^{id} and μ_b^{corr} are the ideal and correlation parts ($b=e,Z,Z-1$). Then the following system of coupled mass action laws can be derived from Eq. (4.9) [23,46,47]

$$n_{Z-1}=\frac{g_{Z-1}}{g_Z}n_Z\exp\left[\frac{1}{k_BT}(E_Z^{ion}+\mu_e^{id}+\mu_e^{corr}+\mu_Z^{corr}-\mu_{Z-1}^{corr})\right]. \tag{4.10}$$

E_Z^{ion} is the ionization energy and g_z denotes the statistical weight. Respective data for carbon and zinc are given in Ref. [42]. The ideal part of the electron chemical potential μ_e^{id} is calculated from $F_{1/2}(\mu_e^{id}/k_BT)=n_e\Lambda_e^3/2$ with $\Lambda_e=\sqrt{2\pi\hbar^2/k_BTm_e}$ being the thermal wavelength and $F_{1/2}$ denotes a Fermi integral. Nonideality effects are accounted for

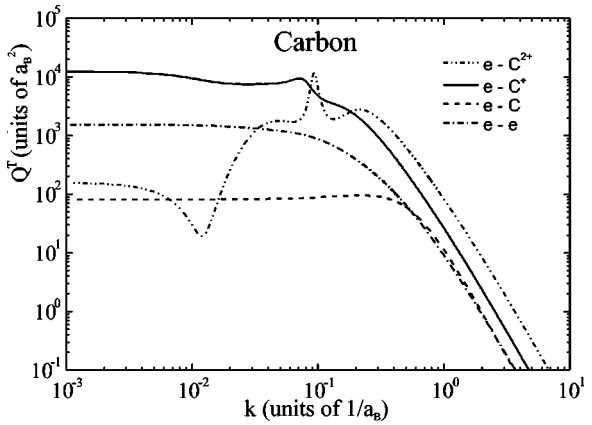

FIG. 9. Transport cross sections for different scattering processes for a given screening parameter $\kappa a_B=0.11$.

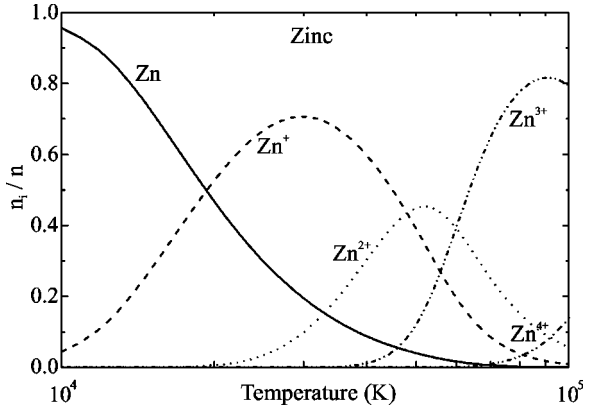

FIG. 10. Composition of zinc plasma as a function of temperature at a given density $n=1.84\times10^{21}$ cm^{-3}. The density is chosen to be in the range of the experiment.

in Eq. (4.10) by the correlation parts of the chemical potentials μ_b^{corr} leading to a lowering of the ionization energy. According to $\mu_b=\partial f/\partial n_b$ we calculated the contributions of the free charged particle interaction to the electron and ion chemical potentials from the Coulomb part of the free energy density f of the plasma. Here, we used Padé interpolation formulas for the electron gas, the ion gas, and the electron-ion interaction contributions determined on the basis of exact quantum statistical results for the low and high density limits as well as Monte Carlo data. The explicit expressions are given in [48,49]. We included the effect of the electron-atom interaction in the μ_b^{corr} on the level of a second virial coefficient in Born approximation using a polarization potential given by Eq. (4.8). Then the corresponding virial coefficient reads $B_{eb}=\int d^3r\, V_{eb}^{pol}(r)$. A further analysis showed that the influence of the atom-atom interaction on the plasma composition could be neglected for the considered plasma parameters. For this estimate we approximated the interatomic potential by a hard-sphere potential with temperature dependent radii [50].

Results for the composition of a zinc plasma as a function of temperature are shown in Fig. 10. The total ion density was chosen to be $n=1.84\times10^{21}$ cm^{-3}, which is in the range of the measured data for the electrical conductivity (see Sec. V). At temperatures below 20 kK a partially ionized plasma is described with atoms, single charged ions, and electrons to be the relevant species. As expected, higher charge states become important at higher temperatures. A remarkable fraction of atoms is described up to temperatures $T=70$ kK. A similar behavior is found for the composition of a carbon plasma. Some calculated data are given in Table I.

Finally, using the results obtained for the plasma composition and the transport cross sections, the electrical conductivity was calculated from Eq. (4.3) for partially ionized carbon and zinc plasmas.

V. THE ELECTRICAL CONDUCTIVITY: EXPERIMENT AND THEORY

The experimental and theoretical results for the electrical conductivity are plotted in Fig. 11 for carbon and in Fig. 12

TABLE I. Plasma composition for a carbon plasma ($Z_A=6$) with a particle density of $n=1.2\times10^{21}$ cm^3 for various plasma temperatures. The fraction of species (C, C^+, C^{2+}) is $\alpha_a=n_a/n$ and the ionization degree is $\alpha_e=n_e/Z_An$.

T (K)	α_C	α_{C^+}	$\alpha_{C^{2+}}$	α_e	σ (S/m)
9000	0.998	0.002		2.45×10^{-4}	2.33×10^{2}
12000	0.987	0.013		2.14×10^{-3}	1.75×10^{3}
16000	0.925	0.075		1.25×10^{-2}	8.51×10^{3}
20000	0.811	0.189		3.14×10^{-2}	1.94×10^{4}
24000	0.672	0.328		5.46×10^{-2}	3.31×10^{4}
30000	0.481	0.517	0.002	8.68×10^{-2}	5.25×10^{4}
39000	0.286	0.698	0.016	1.22×10^{-1}	7.73×10^{4}
50000	0.159	0.766	0.075	1.53×10^{-1}	1.02×10^{5}

for zinc, respectively. Let us begin with the discussion of carbon. From the theoretical results we find the following general behavior of the electrical conductivity for a given temperature: At low densities the conductivity of a plasma consisting of free electrons and ions is described. With increasing number density the formation of neutral atoms occurs. Simultaneously the rate of free electrons is reduced and scattering processes of electrons on atoms become important. Consequently, the electrical conductivity decreases until pressure ionization starts at even higher densities. At this point the conductivity increases rapidly due to the generation of free electrons. A typical minimum behavior of the conductivity occurs, which depends on the number fraction of atoms. In the range of very low temperature and high densities, this behavior is not described completely in the frame of our theoretical model. In particular, the system of mass action laws (4.10) does not give unique results for the degree of ionization at high densities, which indicates the limitations of the partially ionized plasma model used here. In Figs. 11 and 12 results were shown up to densities where the stability condition of the plasma chemical potential is fulfilled and the plasma is in the nondegenerate region. For higher temperatures less atoms are created and the minimum is not distinct. At very high temperatures there are no atoms and the conductivity increases monotonically.

In Fig. 11, measurements are shown for carbon at $T=9$ kK, $T=12$ kK, and $T=16$ kK. The statistical error for the conductivity and the number density is inside the symbol width. As can be seen, the experimental data for $T=16$ kK and for $T=12$ kK at the lower density match the theoretical results well.

For comparison the SESAME data table [31] are presented. There the conductivity calculations are based on an extended Ziman formula. The SESAME data differ from our measurements and calculations by over three orders of magnitude. This can be understood because the Ziman calculation is not valid for this density regime.

For zinc plasmas (Fig. 12) we see the same behavior as

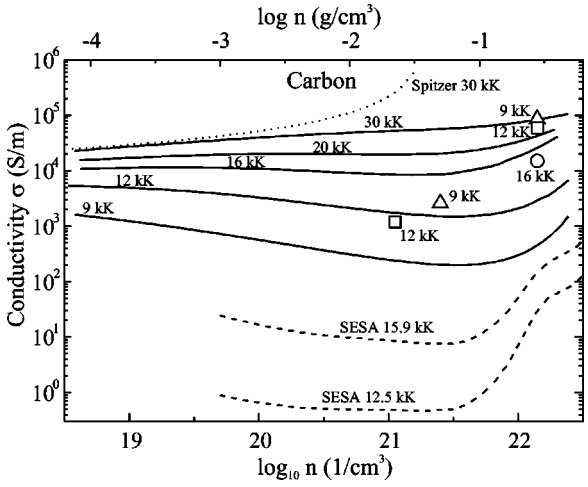

FIG. 11. Electrical conductivity of carbon plasma as a function of density for different temperatures. The measurements are marked as symbols. The experimental data correspond to coupling parameters in the range of $0.3<\Gamma<2.6$. The calculated conductivities are plotted as straight lines. For comparison the SESAME data for 15.9 and 12.5 kK are plotted as dashed lines and the Spitzer result as dotted lines. To calculate the Spitzer conductivity we assume a plasma with electrons and single charged carbon ions.

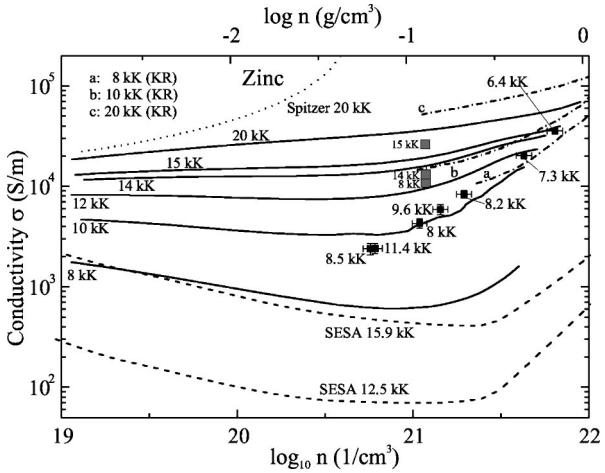

FIG. 12. Electrical conductivity of zinc plasma as a function of density for different temperatures. The measurements are marked as squares. The error bars represent the statistical error of many shots. The gray squares show some older measurements [51]. The experimental data correspond to coupling parameters in the range of $0.7<\Gamma<2.5$. For comparison also the SESAME data are plotted. The calculations of [24] are shown with dashed dotted lines.

for carbon plasmas. The curves for $T=8$ kK, $T=10$ kK, and $T=12$ kK show the limitation of the used plasma model to describe the conductivity in the range of pressure ionization at very high densities. For moderate densities and temperatures, i.e., for nondegenerate plasmas, there is a relatively good agreement between theory and experiment. Especially, for densities of about 10^{21} cm^{-3} and temperatures $T \geqslant 10$ kK the experimental data match the theoretical results well. Here, the kinetic theory applied to a partially ionized plasma gives a reasonable description of the electrical conductivity. Results for the conductivity of zinc in the high density range were given recently by Kuhlbrodt and Redmer using linear respose theory [24]. The results are plotted in Fig. 12 by the dashed-dotted curves neglecting electron-atom scattering. A good agreement with the experimental data follows for low temperatures. Obviously, the theory used in [24] is valid also for the description of the electrical conductivity for the degenerate region of low temperatures and high densities.

As in the case of carbon the SESAME data do not fit the measurements for zinc. Although the deviations are smaller compared to carbon, the SESAME data are not appropriate to describe the electrical conductivity in the considered regime.

The error bars in our measurements represent the statistical error of many shots. The uncertainty of the temperature measurement is about 2 kK. We see this as shown when carrying out many discharges with the same parameters. The cooling effect of the capillary wall is negligible. The temperatures measured in the gap between two capillary pieces and inside one single capillary under the same conditions are the same. However, it is possible that the temperature is higher inside the plasma. On the other hand the temperature measurements of Krisch [18] on aluminum plasmas did not show any temperature gradient in the plasma within the error bars.

VI. CONCLUSIONS

In this paper we present results of electrical conductivity measurements in comparison to calculations for carbon and zinc plasmas in the nonideal plasma range. In the experimental part we describe the production of the plasma by fast wire evaporation and discuss the problems with respect to inhomogeneities. To produce a homogeneous carbon plasma, a special preheating system was employed and the advantage of this system was illustrated by framing and ICCD pictures. With the help of the preheating system it was possible to produce a homogeneous carbon plasma with better quality than metal plasmas in the past. With the use of glass capillaries instabilities were reduced. The temperature was measured spectroscopically by fitting Planck functions to recorded spectra.

In the theoretical part the electrical conductivity for nonideal carbon and zinc plasmas was calculated using quantum kinetic equations applied to a simple plasma model consisting of electrons, ions and atoms. The transport cross sections were calculated on the level of the *T*-matrix approximation using analytic effective two-body interaction potentials. The respective plasma composition was determined from a system of coupled mass action laws where the nonideality was accounted for by the lowering of ionization energies with expressions based on quantum statistical theory.

From the comparison between the experimental data and the theoretical results given in Figs. 11 and 12 we found relatively good agreement in the range of temperatures higher than 10 kK and densities below 10^{22} cm^{-3}. Disagreements are in the region of lower temperatures. The opposite temperature dependence of some experimental data (especially in the region of high densities) compared to the theoretical predictions is not fully understood. Consequently, further experimental and theoretical work has to be done for this region where the transition from the weakly to the fully ionized state due to pressure ionization is expected.

ACKNOWLEDGMENTS

We thank S. Kuhlbrodt and W. D. Kraeft for their discussions and comments on meetings and workshops. We thank the ''Fraunhofer Institut für Lasertechnik'' Aachen, for making available to us their streak and framing camera. This work was supported by the Deutsche Forschungsgemeinschaft (SFB 198 ''Kinetik partiell ionisierter Plasmen'').

[1] L. Spitzer, *Physics of Fully Ionized Gases* (Wiley, New York, 1962).
[2] J.M. Ziman, *Principles of the Theory Of Solids* (Cambridge University Press, London, 1972).
[3] Y.T. Lee and R.M. More, Phys. Fluids **27**, 1273 (1984).
[4] Z. Djurić *et al.*, Phys. Lett. A **155**, 415 (1991).
[5] D.B. Boercker, Phys. Rev. A **23**, 1969 (1981).
[6] F.J. Rogers, H.E. deWitt, and D.B. Boercker, Phys. Lett. A **82**, 331 (1981).
[7] D. Kremp, M. Schlanges, and K. Kilimann, Phys. Lett. A **100**, 149 (1984).
[8] F.F.E. Höhne, R. Redmer, G. Röpke, and H. Wegener, Physica A **128**, 643 (1984).
[9] S. Ichimaru and S. Tanaka, Phys. Rev. A **32**, 1790 (1985).
[10] G. Röpke, Phys. Rev. A **38**, 3001 (1988).
[11] G. Röpke and R. Redmer, Phys. Rev. A **39**, 907 (1989).
[12] H. Reinholz, R. Redmer, and S. Nagel, Phys. Rev. E **52**, 5368 (1995).
[13] J. Starzynski, R. Redmer, and M. Schlanges, Phys. Plasmas **3**, 1591 (1996).
[14] J.F. Benage *et al.*, Phys. Rev. E **49**, 4391 (1994).
[15] J.F. Benage, W.R. Shanahan, and M.S. Murillo, Phys. Rev. Lett. **83**, 2953 (1999).
[16] A.W. DeSilva and H.-J. Kunze, Phys. Rev. E **49**, 4448 (1994).
[17] A.W. DeSilva and J.D. Katsouros, Phys. Rev. E **57**, 5945 (1998).
[18] I. Krisch and H.-J. Kunze, Phys. Rev. E **58**, 6557 (1998).
[19] A. Kloss, T. Motzke, R. Grossjohann, and H. Hess, Phys. Rev. E **54**, 5851 (1996).

[20] A. Kloss, H. Hess, and H. Schneidenbach, High Temp.-High Press. **29**, 215 (1997).
[21] A. Kloss, A.D. Rakhel, and H. Hess, Int. J. Thermophys. **19**, 983 (1998).
[22] H. Hess, A. Kloss, G. Babucke, T. Motzke, and H. Schneidenbach, in *Proceedings of the 4th Asian Thermophysical Properties Conference, Tokyo, Japan, 1995*, edited by A. Nagashima (Keio University, Yokohama, 1995), p. 247.
[23] R. Redmer, Phys. Rev. E **59**, 1073 (1999).
[24] S. Kuhlbrodt and R. Redmer, Phys. Rev. E **62**, 7191 (2000).
[25] R. Scholl and G. Natour, in *Phenomena in Ionized Gases*, edited by K.H. Becker *et al.*, AIP Conf. Proc. 363 (AIP, Woodbury, NY, 1996), p. 373.
[26] R.B. Spielman *et al.*, Phys. Plasmas **5**, 2105 (1998).
[27] S.L. Shapiro and S.A.L. Teukolski, *Black Holes, White Dwarfs and Neutron Stars* (Wiley, New York, 1983).
[28] N.F. Mott and E.A. Davis, *Processes in Non-Crystalline Materials*, 2nd ed. (Clarendon Press, Oxford, 1979), p. 98.
[29] H. Hess, H. Schneidenbach, and A. Kloss, Phys. Chem. Liq. **37**, 719 (1999).
[30] W.E. Forsythe, *Smithsonian Physical Tables*, 9th ed. (Smithsonian Institution, Washington, 1964), p. 394.
[31] *SESAME: The Los Alamos National Laboratory Equation of State Database*, edited by S.P. Lyon and J.D. Johnson (Los Alamos National Laboratory, Los Alamos, NM, 1987).
[32] J. Richter, in *Plasma Diagnostics*, edited by W. Lochte-Holtgreven (North-Holland, Amsterdam, 1968), pp. 1–65; H. Zwicker, *ibid.*, pp. 214–251.
[33] H.R. Griem, *Principles of Plasma Spectroscopy* (Cambridge University Press, Cambridge, 1997).
[34] W. Finkelnburg and H. Maecker, in *Handbuch der Physik*, edited by S. Flügge (Springer-Verlag, Berlin, 1956), Bd. XXII, p. 307.
[35] Yu.L. Klimontovich and D. Kremp, Physica A **109**, 517 (1981).
[36] D. Kremp, M. Schlanges, and Th. Bornath, Phys. Status Solidi B **147**, 747 (1988).
[37] D. Kremp, M. Schlanges, and Th. Bornath, in *The Dynamic of Systems with Chemical Reactions*, edited by J. Popielawski (World Scientific, Singapore, 1989).
[38] M. Schlanges, D. Kremp, and H. Keuer, Ann. Phys. (N.Y.) **41**, 54 (1984).
[39] S. Arndt, F. Sigeneger, F. Bialas, W.D. Kraeft, M. Luft, T. Meyer, R. Redmer, G. Röpke, and M. Schlanges, Contrib. Plasma Phys. **30**, 273 (1990).
[40] H. Schirmer, Z. Phys. **142**, 375 (1955); H. Schirmer and J. Friedrich, *ibid.* **151**, 174 (1958).
[41] R. Redmer, G. Röpke, and R. Zimmermann, J. Phys. B **20**, 4069 (1987).
[42] *CRC Handbook of Chemistry an Physics*, 80th ed., edited by D.R. Lide (CRC Press, London, 1999).
[43] Ch.J. Joachain, *Quantum Collision Theory* (North-Holland, Amsterdam, 1983).
[44] F. Sigeneger, S. Arndt, R. Redmer, M. Luft, D. Tamme, W.D. Kraeft, G. Röpke, and T. Meyer, Physica A **152**, 365 (1988).
[45] D.O. Gericke, S. Kosse, M. Schlanges, and M. Bonitz, Phys. Rev. B **59**, 10 639 (1999).
[46] T. Kahlbaum and A. Förster, Laser Part. Beams **8**, 753 (1990).
[47] W. Ebeling, W.D. Kraeft, and D. Kremp, *Theory of Bound States and Ionization Equilibrium in Plasmas and Solids* (Akademie-Verlag, Berlin, 1976).
[48] W. Ebeling, A. Förster, V.E. Fortov, V.K. Gryaznov, and A.Ya. Polishchuk, *Thermophysical Properties of Hot Dense Plasmas* (Teubner Verlagsgesellschaft, Stuttgart, 1991).
[49] A. Förster, Ph.D. thesis, Humboldt-Universität zu Berlin, 1991.
[50] Landolt-Börnstein, *Zahlenwerte und Funktionen aus Naturwissenschaft und Technik* (Springer-Verlag, Berlin, 1960).
[51] J. Haun, S. Kosse, H.-J. Kunze, M. Schlanges, and R. Redmer, Contrib. Plasma Phys. **41**, 275 (2001).